Energy & Buildings 191 (2019) 200–210

Contents lists available at ScienceDirect

Energy & Buildings

journal homepage: www.elsevier.com/locate/enbuild

Parameter estimation for externally simulated thermal network models☆

O.M. Brastein*, B. Lie, R. Sharma, N.-O. Skeie

Department of Electrical Engineering, Information Technology and Cybernetics, University of South-Eastern Norway, Porsgrunn N-3918, Norway

ARTICLE INFO

Article history:
Received 17 November 2018
Revised 14 February 2019
Accepted 11 March 2019
Available online 11 March 2019

Keywords:
Grey-box models
Stochastic differential equations
Parameter estimation
Profile likelihood
Thermal network models
Unscented Kalman filter
Ensemble Kalman filter

ABSTRACT

Obtaining accurate dynamic models of building thermal behaviour requires a statistically solid foundation for estimating unknown parameters. This is especially important for thermal network grey-box models, since all their parameters normally need to be estimated from data. One attractive solution is to maximise the likelihood function, under the assumption of Gaussian distributed residuals. This technique was developed previously and implemented in the Continuous Time Stochastic Modelling framework, where an *Extended Kalman Filter* is used to compute residuals and their covariances. The main result of this paper is a similar method applied to a thermal network grey-box model of a building, simulated as an electric circuit in an *external tool*. The model is described as a list of interconnected components without deriving explicit equations. Since this model implementation is not differentiable, an alternative Kalman filter formulation is needed. The *Unscented* and *Ensemble Kalman Filters* are designed to handle non-linear models without using Jacobians, and can therefore also be used with models in a non-differentiable form. Both Kalman filter implementations are tested and compared with respect to estimation accuracy and computation time. *The Profile Likelihood* method is used to analyse structural and practical parameter identifiability. This method is extended to compute two-dimensional profiles, which can also be used to analyse parameter interdependence by providing insight into the parameter space topology.

1. Introduction

1.1. Background

The heating and cooling of buildings consumes a significant part of the world's total energy production. While new building materials and techniques may reduce the energy consumption of buildings, the renewal rate of buildings is low [1]. Hence, it is important to study methods that can also reduce energy consumption in existing buildings.

Building Energy Management Systems (BEMS) utilising advanced model-based control methods [2] to forecast the temperature variations of a building in order to predict an optimal sequence of control inputs is a promising method for the reduction of energy consumption. Since the model's prediction accuracy directly influences the efficiency of such methods, it is important to develop accurate models of building thermal behaviour. In addition to describing the time evolution of the system states and outputs, a good model must accommodate descriptions of both measurement noise and process noise [3,4]. This requires a statistically solid framework for estimating unknown parameters [5].

Thermal network models are often used to model the thermal behaviour of buildings [1,6–8]. Implemented as Resistor–Capacitor equivalent circuits, these models offer an intuitive model design based on a cognitive understanding of the thermal physics involved. Since, typically, all parameters of such models must be identified from data, it is important to investigate parameter identifiability prior to assuming physical interpretation of the estimated parameter values [8].

1.2. Previous work

1.2.1. Modelling of dynamic systems

Models are sometimes classified based on the level of physical insight used in their derivation. If the model is mechanistic, i.e., based purely on physical equations, it is classified as *white-box*. Such models excel at describing non-linear state transitions and

☆ This research did not receive any specific grant from funding agencies in the public, commercial or not-for-profit sectors.

* Corresponding author.
E-mail address: ole.m.brastein@usn.no (O.M. Brastein).

https://doi.org/10.1016/j.enbuild.2019.03.018

measurements. They also tend to generalise well between similar systems [5,9]. An alternative approach is the use of *system identification* (SID) methods [3,4,10–12], where a predetermined model structure with unknown coefficients is calibrated using measurements of the system inputs and outputs. This results in a *black-box* model in which no prior physical insight is used, except in the choice of input and output measurements, sample time, and the approximate model complexity. These models tend to have better prediction accuracy, but less capability to generalise [5,9]. SID methods tend to provide better statistics on the model uncertainty, which are typically computed during the calibration process [3–5].

A third, intermediate, possibility is the *grey-box* model, which is based on a simplified model structure constructed using *naive* physical knowledge of the system. Model parameters are calibrated from measurements of the system, similarly to black-box models. Grey-box models are often treated in a stochastic framework [5]. It could be argued that most white-box models include some approximations and/or need calibration of certain parameters. Hence, they can benefit from the application of stochastic grey-box calibration methods. This approach has indeed been claimed as a natural framework for modelling dynamic systems in general [13].

1.2.2. The CTSM framework

Estimation of parameters is essentially an optimisation problem, which requires a well-defined objective function. Several alternatives are used in the literature, such as the deterministic simulation error approach [1]. A statistically solid alternative for stochastic grey-box models is found in [5,14], which is based on maximising the likelihood function evaluated by computing residuals in a Kalman Filter. This method has been previously developed in a number of publications [5,14–16] and implemented in the Continuous Time Stochastic Modelling (CTSM) framework [15]. In CTSM, the residuals needed to evaluate the likelihood function are computed using an *Extended Kalman Filter* (EKF) with subsampling of the *state transition* equations to improve response to non-linear models [5,15]. The EKF is based on linearising the state transitions and/or measurement equations, which requires that the model equations are differentiable [17–19].

1.2.3. Identifiability

Since thermal network building models are partially based on physical knowledge, it is often suggested that the parameters can be assigned a physical interpretation [1,5,6]. This assumption should, however, be verified in the context of parameter identifiability [3,20]. It is well known that models can contain parameters that are structurally non-identifiable [3,20]. Further, lack of proper excitation of the system during data acquisition may lead to practical non-identifiability [3,8,20–22]. While the model structure may be designed such that the parameters are *intended* to have a specific physical meaning, it is not certain that the estimated parameters support this assumption. A good tool for identifiability analysis is the profile likelihood method [8,21,22].

1.3. Overview of paper

In this paper, a resistor-capacitor equivalent thermal network model of a building is expressed as a list of interconnected electrical components. The model is simulated in an external tool without deriving explicit model equations, hence the model cannot be differentiated. This is motivated by the need to simplify experimentation with different model structures in a way that could potentially be automated. The parameter estimation method from the CTSM framework is adapted to non-differentiable models, which requires an alternative to the EKF for computing residuals. Both *the Unscented Kalman Filter* (UKF) [18] and *Ensemble Kalman Filter* (EnKF) [23] are compared and considered for the estimation of residuals. The explicit model equations are also derived on standard linear form, and used with a standard Kalman Filter as a baseline for comparison. Observe that while the model used here is linear, the method is not restricted to linear models; the externally simulated state transitions could well be non-linear.

A profile likelihood approach is used [22] to analyse parameter identifiability. The method is extended to create two-dimensional profiles in the form of *topological heat maps*. These 2D plots are computed for all combinations of parameters. In addition to diagnosing the identifiability of the parameters, these plots allow detection of parameter interdependence.

The paper is organised as follows. The theoretical basis is discussed in Section 2. The model, external simulator and experimental set-up is presented in Section 3, and the results are presented and discussed in Section 4.

2. Theoretical basis

2.1. Stochastic model parameter estimation

Estimation of parameters for a known model structure [17] can be defined as solving the optimisation problem:

$$\hat{\theta} = \arg\min_{\theta} g(\theta; \mathcal{M}, \mathcal{K}, \mathcal{A}) \tag{1}$$

$$s.t.\ \theta \in \Theta$$

Here, $\mathcal{M}$ is a predetermined model structure, which is parametrised by $\theta \in \Theta$, where $\Theta \subseteq \mathbb{R}^{n_\theta}$ is a set of feasible values for the model parameters that form inequality constraints for the optimisation problem in Eq. (1). $\mathcal{K}$ represents the experimental conditions, including a set of measurements of system inputs and outputs. These measurements are used to evaluate the objective function g when θ is varied over the feasible set Θ by a numerical optimisation algorithm $\mathcal{A}$. In the sequel, the algorithm *Constrained Optimisation By Linear Approximation* (COBYLA) [24] is used. This algorithm is gradient free, hence ideal for solving Eq. (1). COBYLA also supports inequality constraints which can be used to impose the limits of the feasible region Θ on the parameter estimates.

Since the model structure $\mathcal{M}$ is a representation of a system $\mathcal{S}$, it is often assumed that $\mathcal{S} \in \mathcal{M}(\Theta)$ and that consequently there exists a true parameter vector θ^* such that $\mathcal{M}(\theta^*) = \mathcal{S}$. However, this is rarely the case, especially for simplified grey-box models based on a *naive* physical understanding of the system $\mathcal{S}$. Typically, the estimate $\hat{\theta}$ depends on the amount of dynamic information in $\mathcal{K}$, the choice of objective function g, and to some extent on the optimisation algorithm $\mathcal{A}$. Hence, it is necessary to analyse the identifiability of the estimated parameters. This topic is further discussed in Section 2.4.

Next, define the continuous time input $u_t \in \mathbb{R}^{n_u}$ and output $y_t \in \mathbb{R}^{n_y}$, and the corresponding ordered sequences of discrete time measurements u_k and y_k taken from the system $\mathcal{S}$:

$$y_{[N]} = [y_0, y_1, \ldots, y_N] \tag{2}$$

$$u_{[N]} = [u_0, u_1, \ldots, u_N] \tag{3}$$

Here, the integer subscripts $k = 0, 1, \ldots, N$ denote the discrete time sampling instants, and the subscript enclosed in $[\cdot]$ is used to indicate an ordered sequence.

A grey-box model can be expressed as a continuous time stochastic differential equation (SDE) with a discrete time measurement equation; adopting the notation of [5]:

$$dx_t = f(x_t, u_t, t, \theta)dt + \sigma(u_t, t, \theta)d\omega_t \tag{4}$$

$$y_k = h(x_k, u_k, t_k, \theta) + e_k \tag{5}$$

where $t \in \mathbb{R}$ is the time variable and $x_t \in \mathbb{R}^{n_x}$ is the continuous time state vector. The first and second terms in the *state transition* equation, given in Eq. (4), are commonly called the *drift* and

diffusion term, respectively [5,25]. The diffusion term expresses the process noise as the function σ multiplied with the differential of a standard Wiener process ω_t. The discrete time *measurement equation* is given in Eq. (5).

2.2. Maximum likelihood

This section gives a summary of the theoretical basis adopted from the CTSM framework [5,14,15]. The objective function g in Eq. (1) can be derived from the likelihood function, which is defined as the probability of observing the measurement sequence $y_{[N]}$ when θ and $\mathcal{M}$ are known, i.e.:

$$L\left(\theta; y_{[N]}, \mathcal{M}\right) = p\left(y_{[N]}|\theta, \mathcal{M}\right) \tag{6}$$

In the sequel, the model structure $\mathcal{M}$ is implicitly assumed known and omitted from the condition. By application of the rule $P(A \cap B) = P(A|B)P(B)$[25], Eq. (6) can be expanded such that:

$$L\left(\theta; y_{[N]}\right) = \left(\prod_{k=1}^{N} p\left(y_k|y_{[k-1]}, \theta\right)\right) p(y_0|\theta) \tag{7}$$

The diffusion term in Eq. (4), which is assumed to be additive and independent of the state x, is driven by a *Wiener process* whose differential is Gaussian distributed [5]. Hence, it is reasonable to assume that the conditional probabilities in Eq. (7) can be approximated by Gaussian distributions [5,15]. This assumption can be checked during model validation by testing the residuals for normality [3,5]. The likelihood can then be expressed as a multivariate Gaussian distribution [5],

$$L\left(\theta; y_{[N]}\right) = \left(\prod_{k=1}^{N} \frac{\exp\left(-\frac{1}{2}\epsilon_k^T \mathcal{E}_{k|k-1}^{-1}\epsilon_k\right)}{\sqrt{\det\left(\mathcal{E}_{k|k-1}\right)}\left(\sqrt{2\pi}\right)^{n_y}}\right) p(y_0|\theta) \tag{8}$$

A Kalman Filter may be used to estimate the quantities

$$\hat{y}_{k|k-1} = \mathbb{E}\left[y_k|y_{[k-1]}, \theta\right] \tag{9}$$

$$\epsilon_k = y_k - \hat{y}_{k|k-1} \tag{10}$$

$$\mathcal{E}_{k|k-1} = \mathbb{E}\left[\epsilon_k \epsilon_k^T\right] \tag{11}$$

In the CTSM framework, an EKF is used. In Section 2.3 the alternative use of UKF and EnKF is discussed.

Eq. (8) can further be simplified by taking the negative of the logarithm; defining the log likelihood function $\ell(\theta; y_{[N]})$:

$$\ell\left(\theta; y_{[N]}\right) = -\ln\left(L\left(\theta; y_{[N]}\right)\right) \tag{12}$$

The solution to the optimisation problem is not affected since

$$\arg\max_{\theta\in\Theta} L\left(\theta; y_{[N]}\right) = \arg\min_{\theta\in\Theta} \ell\left(\theta; y_{(N)}\right) \tag{13}$$

Table 1
Comparing equations for UKF (left) and EnKF (right).

Definitions and initialisation	
$\zeta_m^{(0)} = \frac{\lambda}{\lambda+n_x}$ $\zeta_c^{(0)} = \frac{\lambda}{\lambda+n_x} + \left(1-\alpha^2+\beta\right)$ $\zeta_m^{(i)} = \zeta_c^{(i)} = \frac{1}{2(\lambda+n_x)}, \quad i \in \{1,\dots,2n_x\}$ $\lambda = \alpha^2(n_x+\kappa) - n_x$	$w_k^{(i)} \sim \mathcal{N}(\bar{w}_k, \mathcal{W}_k), \quad i \in \{1,\dots,n_p\}$ $v_k^{(i)} \sim \mathcal{N}(\bar{v}_k, \mathcal{V}_k), \quad i \in \{1,\dots,n_p\}$ $x_{0|0}^{(i)} \sim \mathcal{N}(\bar{x}_0, X_0), \quad i \in \{1,\dots,n_p\}$
$\hat{x}_{0\|0} = \mathbb{E}[x_0] = \bar{x}_0$ $X_{0\|0} = \mathbb{V}\left[x_0 - \hat{x}_{0\|0}\right] = X_0$	$\hat{x}_{0\|0} = \frac{1}{n_p}\sum_{i=1}^{n_p} x_{0\|0}^{(i)}$ $X_{0\|0} = \frac{1}{n_p-1}\sum_{i=1}^{n_p}\left(x_{0\|0}^{(i)} - \hat{x}_{0\|0}\right)(\dots)^T$
State propagation	
$x_{k\|k-1}^{\{2n_x+1\}} = \varsigma\left(\hat{x}_{k-1\|k-1}, X_{k-1\|k-1}\right)$ $x_{k\|k-1}^{(i)} = f\left(x_{k-1\|k-1}^{(i)}, u_{k-1}, \bar{w}_k\right) \quad i \in \{0,\dots,2n_x\}$ $\hat{x}_{k\|k-1} = \sum_{i=0}^{2n_x} \zeta_m^{(i)} x_{k\|k-1}^{(i)}$ [a] $X_{k\|k-1} = \sum_{i=0}^{2n_x} \zeta_c^{(i)}\left(x_{k\|k-1}^{(i)} - \hat{x}_{k\|k-1}\right)(\dots)^T + \mathcal{W}_k$	$x_{k\|k-1}^{i} = f\left(x_{k-1\|k-1}^{(i)}, u_{k-1}, w_{k-1}^{(i)}\right) \quad i \in \{1,\dots,n_p\}$ $\hat{x}_{k\|k-1} = \frac{1}{n_p}\sum_{i=1}^{n_p} x_{k\|k-1}^{(i)}$ [b] $X_{k\|k-1} = \frac{1}{n_p-1}\sum_{i=1}^{n_p}\left(x_{k\|k-1}^{(i)} - \hat{x}_{k\|k-1}\right)(\dots)^T$
Measurement estimate	
$x_{k\|k-1}^{\{2n_x+1\}} = \varsigma\left(\hat{x}_{k\|k-1}, X_{k\|k-1}\right)$ $y_{k\|k-1}^{(i)} = h\left(x_{k\|k-1}^{(i)}, u_{k-1}, \bar{v}_k\right) \quad i \in \{0,\dots,2n_x\}$ $\hat{y}_{k\|k-1} = \sum_{i=0}^{2n_x} \zeta_m^{(i)} y_{k\|k-1}^{(i)}$	$y_{k\|k-1}^{(i)} = h\left(x_{k\|k-1}^{(i)}, u_{k-1}, v_{k-1}^{(i)}\right) \quad i \in \{1,\dots,n_p\}$ $\hat{y}_{k\|k-1} = \frac{1}{n_p}\sum_{i=1}^{n_p} \hat{y}_{k\|k-1}^{(i)}$
Innovation and cross covariance	
$Z_{k\|k-1} = \sum_{i=0}^{2n_x} \zeta_c^{(i)}\left(x_{k\|k-1}^{(i)} - \hat{x}_{k\|k-1}\right)\left(y_{k\|k-1}^{(i)} - \hat{y}_{k\|k-1}\right)^T$ [a] $\mathcal{E}_{k\|k-1} = \sum_{i=0}^{2n_x} \zeta_c^{(i)}\left(y_{k\|k-1}^{(i)} - \hat{y}_{k\|k-1}\right)(\dots)^T + \mathcal{V}_k$	$Z_{k\|k-1} = \frac{1}{n_p-1}\sum_{i=1}^{n_p}\left(x_{k\|k-1}^{(i)} - \hat{x}_{k\|k-1}\right)\left(y_{k\|k-1}^{(i)} - \hat{y}_{k\|k-1}\right)^T$ $\mathcal{E}_{k\|k-1} = \frac{1}{n_p-1}\sum_{i=1}^{n_p}\left(y_{k\|k-1}^{(i)} - \hat{y}_{k\|k-1}\right)(\dots)^T$
$K_k = Z_{k\|k-1}\mathcal{E}_{k\|k-1}^{-1}$	$K_k = Z_{k\|k-1}\mathcal{E}_{k\|k-1}^{-1}$
Aposteriori update[c]	
$\epsilon_{k\|k-1} = y_k - \hat{y}_{k\|k-1}$ $\hat{x}_{k\|k} = \hat{x}_{k\|k-1} + K_k\epsilon_{k\|k-1}$ $X_{k\|k} = X_{k\|k-1} - K_k\mathcal{E}_{k\|k-1}K_k^T$	$x_{k\|k}^{(i)} = x_{k\|k-1}^{(i)} + K_k(y_k - y_{k\|k-1}^{(i)}) \quad i \in \{1,\dots,n_p\}$ [b] $\hat{x}_{k\|k} = \frac{1}{n_p}\sum_{i=n_p}^{n_p} x_{k\|k}^{(i)}$ [b] $X_{k\|k} = \frac{1}{n_p-1}\sum_{i=1}^{n_p}(x_{k\|k}^{(i)} - \hat{x}_{k\|k})(\dots)^T$

[a] Assuming affine noise. (See Remark 3).
[b] Can be omitted (See Remark 5).
[c] Mathematically equivalent but *not* interchangable (See Remark 6).

Finally, by conditioning on knowing y_0, and eliminating the scaling constants $\frac{1}{2}$ from $\ell(\theta;\theta;y_{[N]})$, the objective function from Eq. (1) is given as:

$$g(\theta;\mathcal{M},\mathcal{K}) = \sum_{k=1}^{N} \epsilon_k^T \mathcal{E}_{k|k-1}^{-1} \epsilon_k + \ln\left(\det\left(\mathcal{E}_{k|k-1}\right)\right) \tag{14}$$

where the constant term $c = N \cdot n_y \cdot \ln(2\pi)$ is dropped.

2.3. Alternative KF formulations

The popularity of the Kalman Filter has led to a number of adaptions. The *Extended Kalman Filter* (EKF) is perhaps the most common such adaption and is used in [5]. In the sequel, two other well known KF variations are outlined; the *Unscented Kalman Filter* (UKF) [18] and the *Ensemble Kalman Filter* (EnKF) [23]. In addition to better approximations for non-linear models, UKF and EnKF dispense with the computation of Jacobians and therefore do not require the model to be differentiable [18]. Both filters are listed and compared in Table 1.

Given the SDE for the state transition as in Eq. (4), the time evolution of the probability density function (pdf) of the state, $p(x, t)$, is described by the *Fokker–Planck equation* [23], also known as the *Kolmogorov forward equation* [5]. The multi-dimensional Fokker–Planck equation [25] can be expressed as

$$\frac{\partial p(x,t)}{\partial t} + \sum_i \frac{\partial}{\partial x_i}\left(f_i(x_t,u_t,t,\theta)p(x,t)\right) = \frac{1}{2}\sum_{i,j}\frac{\partial^2}{\partial x_i \partial x_j} p(x,t)\left(\sigma W \sigma^T\right)_{ij} \tag{15}$$

where f_i is the ith component of the state transition model.

In the EKF, the linearised model is used to approximate the first moments of this pdf [23] by a Taylor series expansion truncated after the first term [17,19]. In both UKF and EnKF, the Fokker–Planck equation is instead solved by approximating the solution to Eq. (15) using a set of state realisations. The key difference between the UKF and EnKF is in how that set is constructed. The UKF draws its state realisation set, called *sigma points*, using the unscented transform (UT). The UT of an expected state $\bar{x}$ with covariance X deterministically computes a set of sigma points $x^{\{N\}} = \left\{x^{(i)} : \quad i = 0, 1, \ldots, N\right\}$, where the shorthand $\{\cdot\}$ superscript indicates a set and a superscript $(\cdot)$ denotes a member. For convenience of notation, a UT operator $\varsigma(\bar{x}, X)$ that returns a set of $N = 2n_x + 1$ sigma points is defined as

$$x^{(0)} = \hat{x} \tag{16}$$

$$x^{(i)} = \hat{x} + \left(\sqrt{(n_x+\lambda)X}\right)_i, \; i \in \{1,\ldots,n_x\} \tag{17}$$

$$x^{(n_x+i)} = \hat{x} - \left(\sqrt{(n_x+\lambda)X}\right)_i, \; i \in \{1,\ldots,n_x\} \tag{18}$$

The square root is often implemented using a Cholesky decomposition, and the subscript i denotes the i-th column [17,18]. Note that there are different versions of the UT [3,19], where the one presented in Eqs. (16)–(18) is used in the sequel. For a Gaussian random variable (GRV), the UT is known to approximate the pdf $p(x, t)$ to third order accuracy, and to the second order for non-Gaussian random variables [17]. The introduction of $\lambda = \alpha^2(n_x + \kappa) - n_x$ in Eqs. (16)–(18) gives a set of tuning parameters that can improve approximations of higher order moments [17–19].

In contrast to the deterministic UT, the EnKF represents the state pdf using a Monte Carlo (MC) sampling method [17,18,23]. The pdf is approximated as $p(x,t) = \frac{dN}{n_p}$, where dN is the number of state realisations in some small unit volume and n_p is the total number of realisations [23]. The set of realisations, i.e., the ensemble, is initially drawn at random using the mean and covariance of the initial state. Subsequently, each realisation is propagated as a distinct trajectory, thus making the EnKF equivalent to using a Markov Chain Monte Carlo (MCMC) method to solve the Fokker–Planck equation [23].

2.3.1. Remarks to Table 1

Remark 1. Initialisation for both filters is equivalent if n_p is "large", since the computed ensemble values based on MC sampling converge to the expectation values $\bar{x}_0$ and X_0.

Remark 2. In the UKF, the sigma transform is applied twice to compute the sigma points for both apriori and aposteriori state and covariance estimates. In the EnKF, the realisations are drawn only in the initialisation, and subsequently propagated independently.

Remark 3. The process noise $w_k \sim \mathcal{N}(\bar{w}_k, \mathcal{W}_k)$ and measurement noise $v_k \sim \mathcal{N}(\bar{v}_k, \mathcal{V}_k)$ enter the UKF and EnKF in different ways. The model in Eqs. (4) and (5) assumes affine noise, hence the noise covariances are added to the respective propagation equations in the UKF. For non-affine noise, there are other adaptions of the UKF, e.g., estimating noise by augmenting the state vector, that can be used [18]. In the EnKF, a random number generator (RNG) is used to draw instances of the noise which is subsequently used in the state transition and measurement equations for propagation of the ensemble.

Remark 4. If $\zeta_m^{(i)} = \frac{1}{n_p}$ and $\zeta_c^{(i)} = \frac{1}{n_p - 1}$ in the UKF formulation, the corresponding equations for estimating mean and covariance from the realisation set would be identical to EnKF (except for the iteration index) when n_p is large and $\lambda = 0 \leftrightarrow \alpha = 1, \kappa = 0$.

Remark 5. In order to show the similarity of UKF and EnKF, both filters are formulated with expressions for computing apriori and aposteriori covariance for the state estimate. Observe that for the UKF these are needed in order to compute new sets of sigma points, while in the EnKF this computation can be omitted. Indeed, a fundamental advantage of the EnKF is that it does not require explicit computation of the apriori and aposteriori state estimate covariance matrices, but rather propagates them as approximations in the ensemble. This is an advantage of the EnKF for models with a high number of states.

Remark 6. The EnKF aposteriori update of state realisations and covariance can be shown to be equivalent to the corresponding aposteriori update in the UKF. However, since EnKF treats the set of realisation as independent state trajectories, the ensemble must be updated from apriori to aposteriori state estimates. Hence, the two formulations are not interchangeable, despite being mathematically equivalent.

Remark 7. UKF has three hyper parameters, α, κ and β; default tunings are suggested for standard noise models in the UKF literature. The EnKF has only one hyper parameter: the number of realisations n_p.

2.4. Profile likelihood

Parameter estimates are often reported as a point in the parameter space Θ, or as a *confidence interval* [26] with some stated confidence α. An alternative solution is to present the distribution of the parameters over the feasible range Θ. Since the estimation of parameters is based on the *likelihood function* in Eq. (6), one attractive choice for creating parameter distributions is the *profile likelihood* (PL) method presented in [8,21,22]. This approach was also suggested by the authors of CTSM [27,28]. The PL method explores the parameter space by optimising the parameters in two steps,

rather than simultaneously as in Eq. (1). For simplicity of notation, the dependence on $y_{[N]}$ is omitted from the log likelihood function $\ell(\theta; y_{[N]})$ in the sequel. The *profile likelihood* $\ell_{\mathrm{PL}}(\theta_i)$ is defined as the minimum log likelihood for θ_i when the remaining parameters are freely optimised [22,29]:

$$\ell_{\mathrm{PL}}(\theta_i) = \min_{\theta_{j\neq i}} g\left(\theta_{j\neq i}; \mathcal{M}, \mathcal{K}, \theta_i\right) \tag{19}$$

Values of θ_i must be chosen prior to optimising the remaining $\theta_{j\neq i}$ [22]. A straightforward solution, if the objective function g is well behaved within the constraints of Θ, is to use a *brute force* approach with an even sampling of θ_i. Alternatively, a two-sided gradient decent algorithm, using a freely optimised parameter vector as a starting point, can be applied [22,30]. The resulting likelihood distribution can be plotted as a function of θ_i and subsequently analysed according to the definitions of structural and practical identifiability for *likelihood-based confidence intervals* [8]. Unlike the asymptotic confidence interval, which is based on the curvature of the likelihood function by computation of the Hessian [8,22], the likelihood-based confidence interval is computed by applying a *threshold* to the likelihood function to compute a confidence region [22,29]. Let

$$\left\{\theta : \ell(\theta) - \ell\left(\hat{\theta}\right) < \Delta_\alpha\right\}, \quad \Delta_\alpha = \chi^2(\alpha, n_{\mathrm{df}}) \tag{20}$$

where $\hat{\theta}$ is a freely estimated, presumed optimal, parameter vector, and the threshold Δ_α is the α percentile of the χ^2-distribution with n_{df} degrees of freedom. It follows from *Wilks' theorem* [31] that the logarithm of the likelihood ratio Λ test statistic

$$2\ln(\Lambda) = 2\ln\left(\frac{L(\theta)}{L\left(\hat{\theta}\right)}\right) = \ell(\theta) - \ell(\hat{\theta}) \tag{21}$$

can be used to compare two models. The difference in log likelihood $\ell(\theta) - \ell\left(\hat{\theta}\right)$ is asymptotically χ^2-distributed [22,32], with n_{df} equal to the difference in the number of free parameters between θ and $\hat{\theta}$. Hence, the PL method uses a χ^2 threshold with $n_{\mathrm{df}} = 1$. This form of confidence interval allows interpretation of structural and practical identifiability by inspection of the upper and lower confidence boundaries [22]. If $\ell(\theta)$ is lower than the threshold in both directions, i.e., the interval at the stated confidence level is unbounded ($\pm\infty$), the parameter is classified as structurally non-identifiable [22]. If $\ell(\theta)$ is bounded in one direction, this indicates practical non-identifiability [22,29]. Profile likelihood plots are interpreted similarly. If the plot is lower than the confidence threshold in both directions or only one, this indicates structural or practical non-identifiability, respectively.

2.4.1. Two-dimensional profile likelihood

The PL method essentially projects the n_θ dimensional space Θ onto the single parameter θ_i, by freely estimating the remaining parameters. Hence, if parameters are not independent, the PL method tends to overestimate the width of the likelihood-based confidence interval. A step towards remedying this issue is to modify the PL method to hold out *two* parameters rather than one, i.e.,

$$\ell_{\mathrm{PL2}}\left(\theta_i, \theta_j\right) = \min_{\theta_{k\neq i,j}} g\left(\theta_{k\neq i,j}; \mathcal{M}, \mathcal{K}, \theta_i, \theta_j\right) \tag{22}$$

This results in a two-dimensional distribution which can be analysed in a similar way to the one-dimensional PL [22], using the definition in Eq. (20). The PL2 results are plotted as topological surfaces [22]. This projects the parameter space Θ onto the plane of θ_i and θ_j. In addition to diagnosing identifiability issues, these plots can be used to diagnose parameter interdependence. Observe that since $\hat{\theta}$ has n_θ free parameters while the PL2 estimate has $n_\theta - 2$, this gives $n_{\mathrm{df}} = 2$ for the computation of Δ_α from the χ^2-distribution in Eq. (20).

Applying a confidence threshold to the PL2 method produces *confidence regions* in the (θ_i, θ_j) plane, rather than *intervals* in a single parameter. Based on confidence thresholds computed from the χ^2 distribution, a similar interpretation of these two-dimensional topologies can be applied to diagnose identifiability by requiring that the region is bounded in all directions. If there is an unbounded equipotential *valley* with a log likelihood below the Δ_α threshold, the parameter is structurally non-identifiable. If the interval or region is unbounded only in one direction, this indicates a practically non-identifiable parameter. Examples of two-dimensional PL plots are given in Section 4. If parameter interdependence is observed, re-parametrisation of the model such that the interdependency is resolved, may be advisable in order to obtain a model with tighter confidence bounds on the estimated parameters.

2.4.2. Interpretation of wide confidence regions

It can be argued that a *wide* confidence region is indicative of an identifiability issue even if the region is bounded. If the range of acceptable parameter values is large, the interpretation of the estimated parameters as being determined by the physical properties of the system, i.e., $\mathcal{S} \in \mathcal{M}(\Theta) \to \mathcal{M}\left(\hat{\theta}\right) \approx \mathcal{S}$, is questionable.

One possible cause of wide confidence bounds on the estimated parameters is the presence of nuisance parameters, i.e., parameters whose value is insignificant for the model estimates.

2.4.3. Effect of constrained parameters

Observe that solving the two-step optimisation problem in Eq. (19) subjected to the constraint $\theta \in \Theta$ imposes a restriction on the identified profile $\ell_{\mathrm{PL}}(\theta_i)$. This constraint may skew the results, since the remaining parameters $\theta_{i\neq j}$ are only considered within the region Θ. If parameters are not independent, the profile of one parameter may be influenced by the constraints of another. In the PL2 method, the effect of constrained optimisation of parameters is easier to diagnose, since dependent parameters can be identified from the topology plots.

2.5. Model validation

The CTSM method requires evaluation of the residuals to verify that the assumption of Gaussian distributed residuals is justified [5,15]. In the CTSM literature, the autocorrelation function (ACF) is used to test for normality of residuals in the time-domain, while a cumulative periodogram (CP) is used in the frequency domain [5,8,15]. There are also a number of alternative tests for normality that can be applied, such as the *zero-crossings* test or the *Kolmogorov–Smirnov* test [3].

3. Case study model and simulation

3.1. Model

A thermal network model of a building can be expressed as a resistor-capacitor (RC) circuit. These models are based on a *naive* physical understanding of temperature variations in the building structure, which entails simplifications that necessarily introduce modelling errors. The result is a simplified, lumped parameter model, which should be treated in the framework of grey-box modelling, and hence formulated as stochastic differential equations (SDE) as in Eq. (4) [5].

Fig. 1 shows an example of a candidate RC model which was developed to approximate the thermal behaviour of the experimental building discussed in Section 3.2, partially based on the

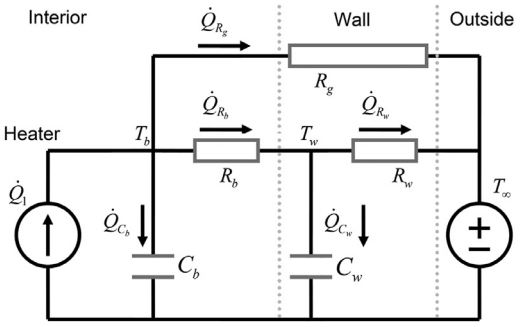

Fig. 1. The R3C2 thermal network model of an experimental building can be expressed as a resistor–capacitor equivalent circuit containing three resistors and two capacitors.

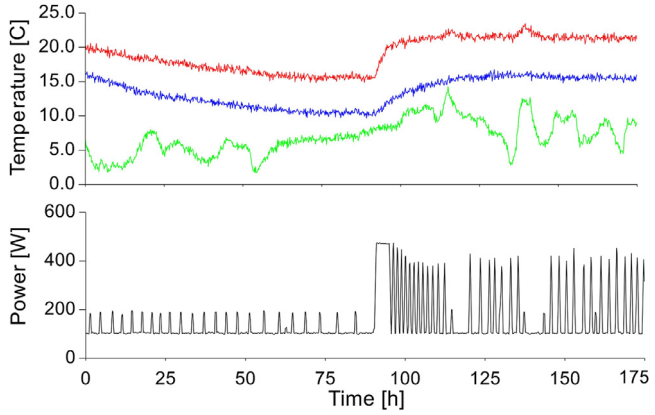

Fig. 2. Calibration data for the R3C2 model. The model outputs T_b (red) and T_w (blue) are plotted together with the outdoor temperature input T_∞ (green). The input power $\dot{Q}$ is plotted separately. (For interpretation of the references to colour in this figure legend, the reader is referred to the web version of this article.)

Table 2
Nominal parameter values and min/max limits for resistances [K/W] and capacitances [J/K].

	R_b	R_w	R_g	C_b	C_w
θ_0	0.100	0.100	0.250	1200k	1200k
θ_{min}	0.030	0.030	0.075	360k	360k
θ_{max}	0.170	0.170	0.425	2040k	2040k

R4C2 model presented in [1]. The model has two outputs: the room temperature T_b and the wall surface temperature T_w, and two inputs: the consumed power by an electric heating element $\dot{Q}$ and the outside temperature T_∞. Five components form the model structure: the thermal resistance between room air and wall R_b, the building envelope R_w, and the thermal resistance of windows and doors R_g. The two capacitances C_b and C_w represent the thermal capacitance of the building interior and envelope, respectively. A nominal parameter vector θ_0, listed in Table 2, is used as the initial value for parameter estimation. Additionally, the feasible values region Θ is limited by θ_{min} and θ_{max}, which are chosen as $0.3 \times \theta_0$ and $1.7 \times \theta_0$, respectively.

3.2. Calibration data

The calibration data used for parameter estimation was obtained from an experimental building located at Campus Porsgrunn of the University of South–Eastern Norway (USN). The data was collected by multiple data acquisition systems, each producing a separate data subset, and combined into a consistent dataset in the preprocessing step. The data was first filtered to remove noise and subsequently resampled into a uniform temporal scale. In order to maintain measurement uncertainty after preprocessing, a random noise component of covariance 0.1 was added to the temperature measurements. The resulting data is presented in Fig. 2.

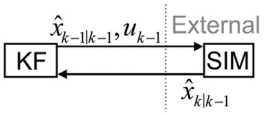

Fig. 3. Illustration of Kalman Filter (KF) with externally simulated (SIM) state propagation.

3.3. RCSimulator

The choice of model structure for a thermal network model, i.e., the RC circuit, usually involves significant experimentation [1,7,16]. To simplify, and possibly automate, the process of finding appropriate model structures, it is useful to simulate such models without requiring explicit model equations. Since the thermal networks are modelled as RC circuits, it is natural to look to the electronics field where circuits are often simulated using tools such as SPICE [33]. A circuit simulator can be used to propagate the state, hence replacing the *drift* term of Eq. (4), as illustrated in Fig. 3. Using this setup with the parameter estimation method in Section 2.2 requires a KF implementation that can handle non-differentiable models, such as UKF and EnKF.

A simple circuit simulator is constructed, named *RCSimulator* for reference in the sequel. Circuit simulators typically define the circuit model as a list of interconnected components, which can be taken directly from the schematic in Fig. 1. By convention, all components have two terminals named *in* and *out*. Each node is assigned an integer index which is used to configure the connections of the components as a circuit. For example, letting node T_b have index 1 and T_w index 2, the component R_b would have input/output assignment (1,2). For each node in the circuit, *Kirchoff's node current law* is used to balance the flow in and out of the node [34]. The system of node equations can be written in difference form:

$$Ax_k + A_m x_{k-1} + Bu_k = 0 \tag{23}$$

The contributions from all components are summed together, such that rows i in A, A_m, and B constitute the balance equation for node i. Eq. (23) is solved for x_k at each time-step in order to propagate the state. The only dynamic element is the capacitor, which is implemented using an implicit Euler discretisation, $\left(\frac{dx}{dt}\right)_{t_k} \approx \frac{x_k - x_{k-1}}{\Delta t}$, by contributing to both the A and A_m matrices. Voltage sources are implemented as constraints on the difference between the states of the two connected nodes. The measurement Eq. (5) can be implemented as measuring the potential between selected nodes in the RC circuit.

The simulation scheme, and in particular the discretisation of the capacitive elements, could be extended with more accurate approximations such as the *Runge–Kutta 4th order* (RK4) scheme [35]. It is also possible to introduce non-linear components, such as variable resistors. Observe that while the test case model used here is linear, the method of estimating residuals with UKF or EnKF for externally simulated models has no such restriction.

3.4. Discrete time linear model

For comparison, the model is also expressed in a standard linear state space form

$$\frac{dx}{dt} = Ax_t + Bu_t + Gw_t \tag{24}$$

where

$$x_t = \begin{bmatrix} T_b \\ T_w \end{bmatrix},\ u_t = \begin{bmatrix} \dot{Q}_1 \\ T_\infty \end{bmatrix},\ B = \begin{bmatrix} \frac{1}{C_b} & \frac{1}{C_b R_g} \\ 0 & \frac{1}{C_w R_w} \end{bmatrix}$$

$$A = \begin{bmatrix} -\frac{1}{C_b R_b} - \frac{1}{C_b R_g} & \frac{1}{C_b R_b} \\ \frac{1}{C_w R_b} & -\frac{1}{C_w R_b} - \frac{1}{C_w R_w} \end{bmatrix}$$

and $w_t \sim N(0, W)$ is the process noise (model error), W is the spectral density of w_t and G is a noise distribution matrix which is assumed constant. Hence $Gw_t dt$ is equivalent to the stochastic diffusion term $\sigma(u_t, t, \theta)d\omega$ in Eq. (4) such that $GWG^T = \sigma\sigma^T$ [5].

The model in Eq. (24) is written in continuous time and must be discretised for use in a computer KF implementation. Assuming zero order hold (ZOH) on the inputs [36] gives

$$\frac{d}{dt}\begin{bmatrix} x \\ u \end{bmatrix}_t = \begin{bmatrix} A & B \\ 0 & 0 \end{bmatrix}\begin{bmatrix} x \\ u \end{bmatrix}_t + \begin{bmatrix} G \\ 0 \end{bmatrix} w_t \tag{25}$$

The discrete time equivalent system, again assuming ZOH on inputs, gives the difference equation

$$\begin{bmatrix} x \\ u \end{bmatrix}_k = \begin{bmatrix} \tilde{A} & \tilde{B} \\ 0 & 1 \end{bmatrix}\begin{bmatrix} x \\ u \end{bmatrix}_{k-1} + \begin{bmatrix} \tilde{G} \\ 0 \end{bmatrix} w_k \tag{26}$$

where $w_k \sim N(0, \mathcal{W})$ and $\mathcal{W}$ is the process noise covariance. On the interval $[t_{k-1}, t_k[\rightarrow \Delta t = t_k - t_{k-1}$, Eq. (25) has the known solution

$$\begin{bmatrix} x \\ u \end{bmatrix}_{t_k} = \exp\left(\Delta t \begin{bmatrix} A & B \\ 0 & 0 \end{bmatrix}\right)\begin{bmatrix} x \\ u \end{bmatrix}_{t_{k-1}} + \begin{bmatrix} \Delta x_w \\ 0 \end{bmatrix} \tag{27}$$

which by direct comparison with Eq. (26) gives the discrete model matrices $\tilde{A} = e^{A\Delta T}$ as the upper left sub-matrix and $\tilde{B}$ as the corresponding upper right sub-matrix. The diffusion of the states driven by the process noise w_t is here expressed by the term Δx_w which is yet undetermined. $\tilde{G}$ is obtained from the expectation

$$\begin{aligned} E\left(x_{k|k-1}x_{k|k-1}^T\right) &= X_{k|k-1} \\ &= \tilde{A}X_{k-1|k-1}\tilde{A}^T + \int_{t_{k-1}}^{t_k} e^{A\tau} Q_c e^{A^T\tau} d\tau \end{aligned} \tag{28}$$

where $Q_c = GWG^T$. This integral can be solved using the Van Loan method in [37]. Let

$$D = \exp\left(\Delta t \begin{bmatrix} -A & Q_c \\ 0 & A^T \end{bmatrix}\right) = \begin{bmatrix} D_{11} & D_{12} \\ 0 & D_{22} \end{bmatrix} \tag{29}$$

Then

$$Q(\Delta t) = \int_{t_{k-1}}^{t_k} e^{A\tau} Q_c e^{A^T\tau} d\tau = \tilde{G}\mathcal{W}\tilde{G}^T = D_{22}^T D_{12} \tag{30}$$

From Eq. (30) it is possible to compute *either* the process noise covariance $\mathcal{W}$ or the discrete time distribution matrix for the process noise $\tilde{G}$ when the other is known or assumed. Setting $\tilde{G} = I$ gives $\mathcal{W} = Q(\Delta t) = D_{22}^T D_{12}$ which is equivalent to the result in [5]. This is also the form typically used in derivation of Kalman Filters [18,19], as shown in Table 1.

While the primary focus of this paper is on the externally simulated model, the model in Eq. (26) is used as a baseline for comparison with other combinations of Kalman Filter implementations and model discretisation methods. Other approximations for the discrete time model can be found using, e.g., explicit Euler or the RK4 scheme [35].

4. Results and discussion

4.1. Test cases

Multiple combinations of KF implementations and model state propagation methods are tested and compared. The various cases, listed in Table 3, are compared with a baseline (BL) consisting of the linear explicit model from Section 3.4 and a standard KF.

Table 3
Model representation as list of interconnected components.

#	Kalman Filter	Model
BL	KF	Eq. (26) (exact)
1	KF	Eq. (24) (exp. Euler)
2	UKF	RCSimulator
3	UKF	Eq. (24) (RK4)
4	EnKF ($n_p = 50$)	RCSimulator,
5	EnKF ($n_p = 500$)	RCSimulator
6	EnKF ($n_p = 2000$)	RCSimulator
7	EnKF ($n_p = 5000$)	RCSimulator

Table 4
Freely estimated parameters for each case.

#	R_b	R_w	R_g	C_b	C_w	$\Delta\ell$
BL	0.097	0.114	0.136	1642k	1272k	-
1	0.100	0.118	0.134	1653k	1238k	0.22
2	0.101	0.119	0.133	1643k	1220k	−0.44
3	0.100	0.118	0.134	1651k	1228k	−0.11
4	0.075	0.103	0.133	1969k	1493k	121
5	0.093	0.122	0.201	1633k	1571k	32.5
6	0.080	0.100	0.217	1779k	1277k	12.5
7	0.076	0.091	0.190	1961k	1663k	4.51

4.2. Tuning

The covariance matrix for the measurement noise $\mathcal{V} = \text{diag}(0.1, 0.1)$ is obtained from the calibration data in $\mathcal{K}$. The process noise covariance $\mathcal{W}$ is often difficult to estimate, hence it is typically treated as a tuning parameter. By using the model validation results, i.e., testing the normality of the residuals as discussed in Section 4.4, $\mathcal{W} = \text{diag}(0.004, 0.002)$ is found by trial and error. An alternative solution is to include the elements of $\mathcal{W}$ in θ and let the optimisation algorithm $\mathcal{A}$ determine them [5], in accordance with Eq. (14).

The UKF and EnKF have some additional tuning parameters. The default UKF settings $\alpha = 10^{-3}$, $\kappa = 0$, $\beta = 2$ as suggested in [17] are used. For the EnKF, the only tuning parameter is the number of realisations n_p for which four different values are used, depending on the test cases given in Table 3.

4.3. Estimated parameters

The parameters are estimated for each test case by minimising Eq. (14) using the residuals and their covariance as obtained from the KF in each case. The results are shown in Table 4. The rightmost column lists the difference in log likelihood, $\Delta\ell$, between each case and the BL.

The estimated parameters $\hat{\theta}$ and corresponding relative log likelihood, $\Delta\ell$, for Cases 1–3 closely match the results computed for the baseline, which indicate that the UKF, combined with either RK4 discretisation or the RCSimulator, correctly estimates the residuals for evaluation of the likelihood function in Eq. (8).

The results for the EnKF Cases 4 to 7 differ significantly more from the BL case, as shown in Table 4. The parameters are different from the BL and also the log likelihood values are significantly higher than for the BL case. They tend towards the BL case as n_p is increased, but at $n_p = 5000$ in Case 7, there is still a significant difference. The EnKF is based on a Monte Carlo approximation of the state distribution $p(x, t)$. Hence, the computed residuals and covariance are also an approximation. This leads to a significant deviation from the BL results. The UKF is known to be exact for linear systems [18], hence no such deviation from the BL is observed for Cases 2 and 3, beyond some small deviations resulting from differences in state propagation approximations.

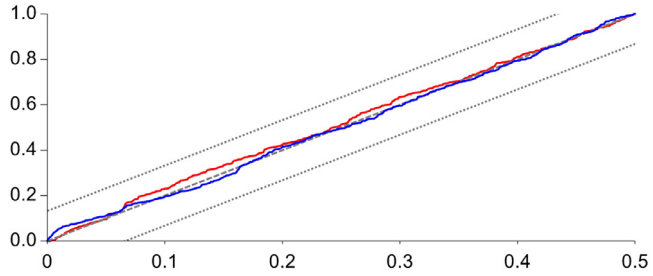

Fig. 4. Cumulative periodogram with 95% confidence bands for the residuals of the outputs T_b (red) and T_w (blue). (For interpretation of the references to colour in this figure legend, the reader is referred to the web version of this article.)

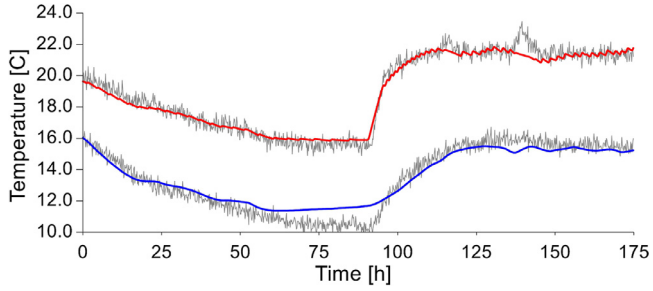

Fig. 5. Deterministic simulation. Measured values (grey) with T_b (red) and T_w (blue). (For interpretation of the references to colour in this figure legend, the reader is referred to the web version of this article.)

Table 5
Testing distribution of residuals for normality.

Output	T_b	T_w
Zero crossing	530	526
Kolmogorov–Smirnov	0.0232	0.0126

4.4. Model validation and normality tests

The use of the likelihood function for parameter estimation is based on the assumption of Gaussian distributed residuals, hence the residuals should be tested for normality in order to verify that assumption [5]. In the sequel, residuals from Case 2 are used, but near identical results are obtained for Cases 1, 3 and BL. Cases 4 to 7 are not considered further in this section. There are several tests that can be used to validate the normality assumption, such as the cumulative periodogram (CP) presented in Fig. 4. Other normality tests are the *zero-crossing count* (ZC) and the *Kolmogorov–Smirnov* (KS) test [3] as listed in Table 5. The *zero-crossing* test for $N = 1050$ samples gives a 95% confidence interval [3] of (493, 556) which covers the test results for both outputs. Similarly, the KS test gives a critical value of 0.0417, which is higher than the score for both outputs. Finally, the CP in Fig. 4 indicates that the residuals are evenly distributed in the frequency domain, hence giving an approximately linear CP within the 95% confidence band [8,14,16,38]. After having tuned the process noise covariance matrix $\mathcal{W}$ by trial and error, these tests indicate that the residuals are well approximated by a Gaussian distribution.

Another method for validation of a model with estimated parameters is to perform a deterministic simulation using measured system inputs [3]. If the parameters are reasonable, the model predictions should approximately agree with the observed output measurements. The results of such a simulation are presented in Fig. 5. As shown, the simulation reproduces the system behaviour from the calibration data reasonably well, which further validates the model and the estimated parameter values.

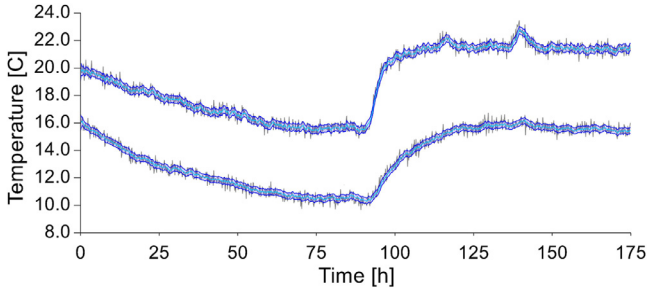

Fig. 6. Results from Case 2, using the UKF with RCSimulator. Observed measurements are plotted in grey, and estimated outputs with two sd error bands in blue: T_b (top) and T_w (bottom). (For interpretation of the references to colour in this figure legend, the reader is referred to the web version of this article.)

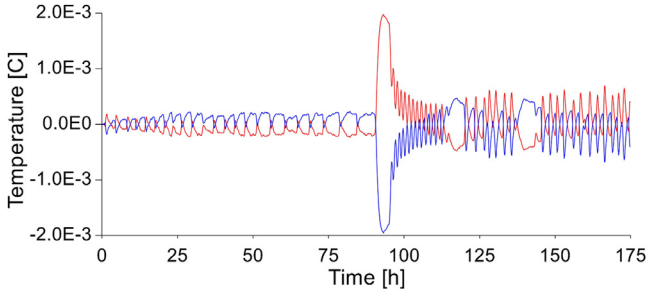

Fig. 7. Difference in output T_b between Case 1 (red) and Case 2 (blue) and the baseline linear KF with exact model discretisation. (For interpretation of the references to colour in this figure legend, the reader is referred to the web version of this article.)

Table 6
Comparing difference with baseline for each case.

#	$RMSE(\Delta\epsilon)$	$RMSE(\Delta\mathcal{E})$	*Runtime*
BL	–	–	1.4 ms
1	7.91×10^{-4}	9.49×10^{-6}	1.7 ms
2	7.79×10^{-4}	9.35×10^{-6}	10.4 ms
3	5.5×10^{-9}	5.77×10^{-13}	9.9 ms
4	1.39×10^{-1}	4.88×10^{-2}	0.092 *s* (0.078 s)
5	4.13×10^{-2}	1.56×10^{-2}	0.88 *s* (0.75 s)
6	2.14×10^{-2}	7.76×10^{-3}	3.5 *s* (3.1 s)
7	1.40×10^{-2}	4.70×10^{-3}	9.2 *s* (7.9 s)

4.5. Comparing Kalman filters

In this section, the results for all cases in Table 3 are compared in detail. First, Fig. 6 shows the estimated output for Case 2 plotted with an error band of two standard deviations together with the measured output. A visual inspection of Fig. 6 shows that the estimated output ± 2 standard deviations (sd) captures most of the variation in the measurements, indicating that the UKF correctly estimates the covariance of the estimated output.

Next, the root mean square error (RMSE) is used to compare the difference between each case and the BL, for both the residuals, $\Delta\epsilon$, and their covariance, $\Delta\mathcal{E}$. The results are presented in Table 6, together with the runtime of each case. For the EnKF, the computation time was measured both with and without (in brackets) computation of apriori and aposteriori covariance.

Several interesting observations can be made from Table 6. First, the quantified RMSE results show that Cases 1 to 3 give similar results to the BL case. In particular, Case 3 is near identical to the BL, with an RMSE around 10^{-9}. This result shows that the UKF gives near optimal estimates, with the deviations mostly explained by approximations introduced by the model discretisation method. Further, the results from EnKF differ significantly, even

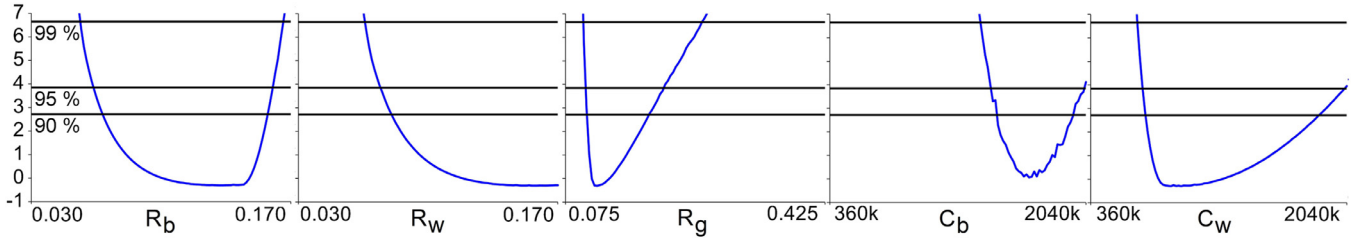

Fig. 8. PL1 method for diagnosing parameter identifiability.

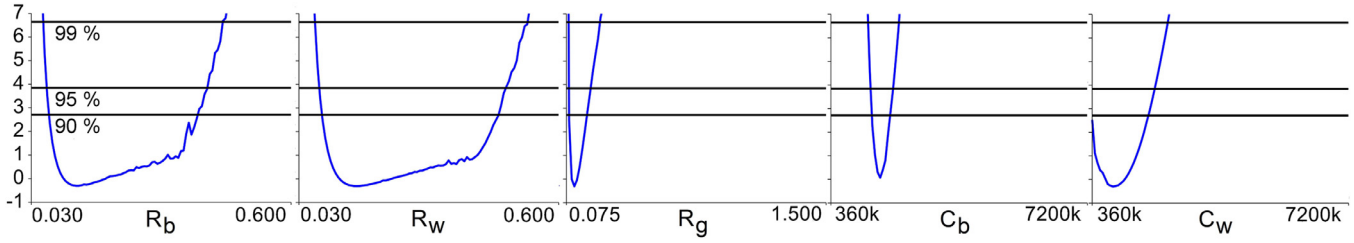

Fig. 9. PL1 method with extended feasible region Θ.

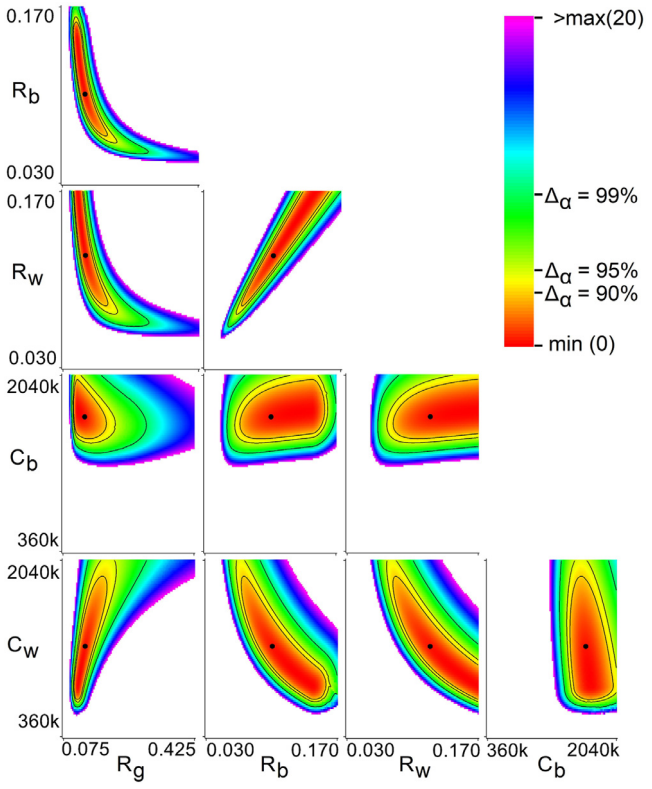

Fig. 10. Heat map with isolines at confidence levels 90%, 95% and 99%, from the PL2 method. The freely optimised solution $\hat{\theta}$ is marked by a black dot in all plots. All plots cover the entire sub-region of Θ for their respective parameters. For reduced clutter, the axis labels are only included on the left-most/lower-most plots. The figure legend shows that the colour red indicates a relative likelihood close to 0, while purple indicates a relative log likelihood of 20. Values above 20 are not plotted, thus highlighting the most interesting region in the parameter space Θ. (For interpretation of the references to colour in this figure legend, the reader is referred to the web version of this article.)

with $n_p = 5000$, from those obtained by KF and UKF, especially for low n_p.

To verify the implementation of the RCSimulator, Cases 1 and 2 are compared in Fig. 7. The error, compared to BL, in residuals of output T_b is similar for Cases 1 and 2, but interestingly with the opposite sign. This is reasonable since Case 1 uses explicit Euler discretisation of the continuous time model, while the RCSimulator, discussed in Section 3.3, uses implicit Euler approximation for the capacitance elements. The output T_w shows the same behaviour.

4.5.1. Computation time

Based on experience with the test case, the objective function is known to be well behaved in Θ, hence, a simple brute force algorithm is used to draw θ_i, and θ_j. With a resolution of 100 steps per parameter, the PL2 method requires 10,000 repeated executions of the parameter estimation algorithm per combination of parameters. With five parameters, there are ten different combinations of parameters which gives a total of 100,000 required executions. Hence, computational time for this method is significant. The evaluation of Eq. (22) can be efficiently parallelised, which reduces computation time. For the test case used in this paper the computation time per PL2 plot is around 30–60 minutes when the UKF is used with the RCSimulator on a six-core CPU. For large number of parameters, the overall computational load may be unpractical. However, if the objective function is smooth in Θ, a lower resolution plot may be sufficient to diagnose parameter identifiability and interdependence issues, or at least identify which parameter combinations may warrant further study with higher resolution. Further improvements in computation time may be achieved by applying faster maximum likelihood estimation algorithms [39].

The runtime of the EnKF, as shown in Table 6, are orders of magnitude slower than the UKF cases, while the UKF cases are only about six times slower than the standard KF cases. Observe also that the overhead of using the external simulator is only around 1 *ms*. Since the EnKF uses a MC sampling of the state distribution $p(x, t)$ in order to solve the Fokker–Planck Eq. (15), a larger number of realisations is required compared with the UKF [23]. The unscented transform used in UKF requires $2n_x + 1$ state realisations. Observe that the computational times in Table 6 are approximately linear in the number of realisations used for both EnKF and UKF. This is expected due to the relative similarities of the two KF implementations as indicated in Table 1. For a simple model such as the thermal network used here, with $n_x = 2$, it is not surprising that UKF far outperforms EnKF in terms of computational efficiency. EnKF was after all designed for large scale systems where n_x is very high.

In the sequel, only the UKF will be considered for further study. As discussed, the PL method requires a large number of repeated parameter optimisations, which in turn require an even larger

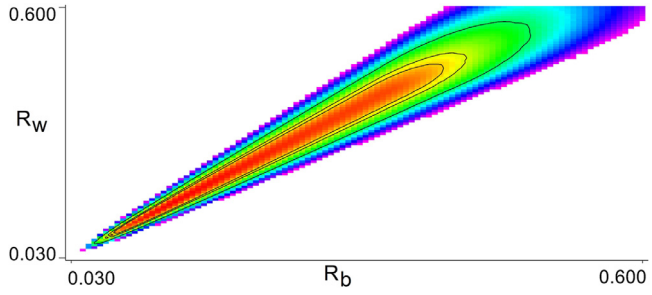

Fig. 11. PL2 topology of R_b vs R_w with extended feasible region Θ.

number of KF executions. Hence, runtime is of critical importance, which excludes the use of EnKF in this case.

4.6. Profile likelihood for Case 2

The theoretical foundation for the *profile likelihood* (PL) method [8,22] is discussed, and extended to simultaneously analysing two parameters in Section 2.4. In the sequel, both PL methods are applied to the R3C2 model from Section 3. Results are obtained using the configuration in Case 2 from Table 3. The log likelihood obtained by freely estimating all parameters is used as a reference, i.e., the plots present $\ell_{\mathrm{PL}}(\theta_i) - \ell\left(\hat{\theta}\right)$.

Fig. 8 shows the parameter profiles from the PL1 method in Eq. (19), with confidence thresholds at stated confidence levels from the χ^2 distribution with $n_{\mathrm{df}} = 1$. The topological surfaces from the PL2 method in Eq. (22) are plotted as heat maps, with isolines at specified confidence levels from the χ^2 distribution with $n_{\mathrm{df}} = 2$, in Fig. 10.

As discussed in Section 2.4, the definition of identifiability used in [22] requires the *likelihood-based confidence interval/region* to be bounded for a prescribed confidence level. Observe from Fig. 8 that four of the parameters have bounded profiles within the feasible region Θ. However, parameter R_w is indicated as practically non-identifiable, since the profile is below the prescribed thresholds in the positive direction. However, the PL analysis is computed subject to the constraint $\theta \in \Theta$. It is not clear from the results if extending the feasible values for R_w would result in a bounded PL also for this parameter. Hence, further examination of R_w by widening the feasible region Θ is required.

The results from PL2 in Fig. 10 show the same pattern of identifiability as for the one-dimensional PL plots. At first glance, the PL2 method confirms that parameter R_w is classified as practically non-identifiable, while R_b has a wide but bounded profile. However, the PL2 method provides additional insight into the parameter domain Θ. Observe from the plot for R_b vs R_w that the shape of the log likelihood function of parameter space $\ell(\Theta)$ projected onto the (R_b, R_w) plane indicates that there is interdependence between these two parameters. By comparing the PL1 plot for R_b to the PL2 plot for R_b vs R_w and projecting the PL2 results onto the R_b axis, it can be observed that the sharp bend in the PL1 Fig. 8 plot is actually a consequence of the constraint on R_w. A similar constraint artefact, a sharp bend near the lower end of the feasible range, can be seen in the PL1 plot for C_w. It is likely that the observed topology from Fig. 10 would be extended if the parameter domain Θ was wider, hence allowing optimal values for R_b to be obtained above the constrained profile observed in Fig. 8.

Further, the topology obtained from PL2 shows that the width of the profile from PL1 is significantly overestimated due to the parameter interdependence. Once either R_b or R_w is obtained, the profile of the other parameter is much narrower than what the PL1 method suggests.

4.6.1. Extending the parameter space

Next, the parameter space Θ is widened by letting the parameters extend to six times the nominal value, e.g., $\theta_{\max} = 6 \cdot \theta_0$. The PL1 results in Fig. 9 now show that all five parameters are identifiable, i.e. the likelihood profiles cross the confidence threshold in both directions. Further, the PL2 result for the parameter combination (R_b, R_w) in Fig. 11 shows that the topology observed in Fig. 10 indeed extends beyond the initial limited parameter space Θ.

5. Conclusion

In this paper, the *Unscented Kalman Filter* (UKF) and the *Ensemble Kalman Filter* (EnKF) have been compared for the purpose of estimating residuals and covariance for evaluation of the likelihood function. The state transition model was implemented in a non-differentiable external simulation tool, hence requiring a Kalman filter implementation other than the *Extended Kalman Filter* (EKF). The results from applying both filters to the parameter estimation problem show that the UKF outperforms the EnKF in both accuracy and computational time for this particular model. Since the UKF requires fewer realisations for few states, this result is expected. The EnKF was developed to handle large scale dynamic systems with a high number of model states and relatively few measurements. Since the underlying case study model is linear, the UKF is optimal, limited only by approximations to the state propagation method in the external simulation tool. For models with a larger number of states the EnKF may well be a better choice.

The use of a UKF allowed the likelihood function to be evaluated even though the thermal network building model was implemented as a non-differentiable external simulator. Comparing the results of the externally simulated component list model with simulations using the explicitly expressed linear equations showed that the results are near identical. While the use of the simulator and a UKF is about six times slower in computational time compared to the explicit model and a standard KF, the external model allows for simple manipulation of the component list model structure. This could potentially be used to automate the construction of thermal network model structures for the thermal behaviour of a specific building prior to parameter estimation.

The profile likelihood (PL) method was applied to the thermal network model to create one- and two-dimensional parameter profile plots. The PL2 plots were used to show that R_b and R_w are interdependent, which caused the PL1 method to overestimate the width of their respective profiles. Further, the interdependence of the parameters also skewed the results of the PL1 method due to the constraints of the feasible parameter region. Based on the PL2 plots, the parameter region was extended, which resulted in improved likelihood profiles also from the PL1 method. The combination of one- and two-dimensional likelihood profiles was shown to provide valuable insight into the parameter domain. These plots show that all of the parameters are identifiable, but with large confidence regions. This indicates lack of dynamic system excitation in the calibration data, which could be remedied by improved experimental design, e.g., use of Pseudo Random Binary Sequence as actuation.

References

[1] T. Berthou, P. Stabat, R. Salvazet, D. Marchio, Development and validation of a gray box model to predict thermal behavior of occupied office buildings, Energy Build. 74 (2014) 91–100, doi:10.1016/j.enbuild.2014.01.038.
[2] M. Killian, M. Kozek, Ten questions concerning model predictive control for energy efficient buildings, Build. Environ. 105 (2016) 403–412, doi:10.1016/j.buildenv.2016.05.034.
[3] R. Johansson, System Modeling and Identification, Information and System Sciences Series, Prentice Hall, 1993.
[4] L. Ljung, System Identification: Theory for the User, Prentice Hall information and System Sciences Series, Prentice Hall PTR, 1999.

[5] N.R. Kristensen, H. Madsen, S.B. Jørgensen, Parameter estimation in stochastic grey-box models, Automatica 40 (2) (2004) 225–237, doi:10.1016/j.automatica.2003.10.001.
[6] S.F. Fux, A. Ashouri, M.J. Benz, L. Guzzella, EKF based self-adaptive thermal model for a passive house, Energy Build. 68 (2014) 811–817, doi:10.1016/j.enbuild.2012.06.016.
[7] G. Reynders, J. Diriken, D. Saelens, Quality of grey-box models and identified parameters as function of the accuracy of input and observation signals, Energy Build. 82 (2014) 263–274, doi:10.1016/j.enbuild.2014.07.025.
[8] A.-H. Deconinck, S. Roels, Is stochastic grey-box modelling suited for physical properties estimation of building components from on-site measurements? J. Build. Phys. 40 (5) (2017) 444–471, doi:10.1177/1744259116688384.
[9] A. Afram, F. Janabi-Sharifi, Gray-box modeling and validation of residential HVAC system for control system design, Appl. Energy 137 (2015) 134–150, doi:10.1016/j.apenergy.2014.10.026.
[10] L. Ljung, Prediction error estimation methods, Circuits Syst. Signal Process. 21 (1) (2002) 11–21, doi:10.1007/BF01211648.
[11] D. Di Ruscio, Combined deterministic and stochastic system identification and realization: DSR–a subspace approach based on observations, Model. Identif. Control 17 (3) (1996) 193–230, doi:10.4173/mic.1996.3.3.
[12] R. Ergon, D. Di Ruscio, Dynamic system calibration by system identification methods, in: Proceedings of the European Control Conference (ECC), IEEE, 1997, pp. 1556–1561.
[13] T. Bohlin, S.F. Graebe, Issues in nonlinear stochastic grey box identification, Int. J. Adapt. Control Signal Process. 9 (6) (1995) 465–490.
[14] H. Madsen, J. Holst, Estimation of continuous-time models for the heat dynamics of a building, Energy Build. 22 (1) (1995) 67–79, doi:10.1016/0378-7788(94)00904-X.
[15] N.R. Kristensen, H. Madsen, Continuous Time Stochastic Modelling-CTSM 2.3., Technical University of Denmark, Lyngby, Denmark, 2003.
[16] P. Bacher, H. Madsen, Identifying suitable models for the heat dynamics of buildings, Energy Build. 43 (7) (2011) 1511–1522, doi:10.1016/j.enbuild.2011.02.005.
[17] E.A. Wan, R. Van Der Merwe, The unscented Kalman filter for nonlinear estimation, in: Proceedings of the IEEE Adaptive Systems for Signal Processing, Communications, and Control Symposium. AS-SPCC., IEEE, 2000, pp. 153–158.
[18] S.J. Julier, J.K. Uhlmann, New extension of the Kalman filter to nonlinear systems, in: Proceedings of the Signal Processing, Sensor Fusion, and Target Recognition VI, 3068, International Society for Optics and Photonics, 1997, pp. 182–194.
[19] D. Simon, Optimal State Estimation: Kalman, H Infinity, and Nonlinear Approaches, John Wiley & Sons, 2006.
[20] C.S. Ferrero, Q. Chai, M. Dueñas Díez, S.H. Amrani, B. Lie, Systematic analysis of parameter identifiability for improved fitting of a biological wastewater model to experimental data, Model. Identif. Control 27 (4) (2006) 219–238, doi:10.4173/mic.2006.4.2.
[21] S.A. Murphy, A.W. Van der Vaart, On profile likelihood, J. Am. Stat. Assoc. 95 (450) (2000) 449–465, doi:10.2307/2669386.
[22] A. Raue, C. Kreutz, T. Maiwald, J. Bachmann, M. Schilling, U. Klingmüller, J. Timmer, Structural and practical identifiability analysis of partially observed dynamical models by exploiting the profile likelihood, Bioinformatics 25 (15) (2009) 1923–1929, doi:10.1093/bioinformatics/btp358.
[23] G. Evensen, The ensemble Kalman filter for combined state and parameter estimation, IEEE Control Systems 29 (3) (2009) 83–104, doi:10.1109/MCS.2009.932223.
[24] M.J. Powell, A direct search optimization method that models the objective and constraint functions by linear interpolation, in: Advances in Optimization and Numerical Analysis, Springer, 1994, pp. 51–67.
[25] A.H. Jazwinski, Stochastic Processes and Filtering Theory, Dover Publications, Inc, 1970.
[26] E.L. Lehmann, G. Casella, Theory of Point Estimation, Springer Science & Business Media, 2006.
[27] R. Juhl, J.K. Møller, H. Madsen, ctsmr-Continuous Time Stochastic Modeling in R. preprint arXiv: 1606.00242, 2016.
[28] R. Juhl, J.K. Møller, J.B. Jørgensen, H. Madsen, Modeling and prediction using stochastic differential equations, in: Prediction Methods for Blood Glucose Concentration, Springer, 2016, pp. 183–209.
[29] D. Venzon, S. Moolgavkar, A method for computing profile-likelihood-based confidence intervals, Appl. Stat. (1988) 87–94, doi:10.2307/2347496.
[30] T. Maiwald, J. Timmer, Dynamical modeling and multi-experiment fitting with potterswheel, Bioinformatics 24 (18) (2008) 2037–2043, doi:10.1093/bioinformatics/btn350.
[31] S.S. Wilks, The large-sample distribution of the likelihood ratio for testing composite hypotheses, Ann. Math. Stat. 9 (1) (1938) 60–62, doi:10.1214/aoms/1177732360.
[32] W.Q. Meeker, L.A. Escobar, Teaching about approximate confidence regions based on maximum likelihood estimation, Am. Stat. 49 (1) (1995) 48–53, doi:10.2307/2684811.
[33] L.W. Nagel, SPICE2: a computer program to simulate semiconductor circuits, Ph.D. dissertation, University of California at Berkeley, 1975.
[34] J.W. Nilsson, Electric Circuits, Pearson Education India, 2008.
[35] C. Runge, Ueber die numerische auflösung von differentialgleichungen, Mathematische Annalen 46 (2) (1895) 167–178, doi:10.1007/BF01446807.
[36] R.A. DeCarlo, Linear Systems: A State Variable Approach with Numerical Implementation, Prentice-Hall, Inc., 1989.
[37] C. Van Loan, Computing integrals involving the matrix exponential, IEEE Trans. Autom. Control 23 (3) (1978) 395–404, doi:10.1109/TAC.1978.1101743.
[38] H. Madsen, Time Series Analysis, Chapman and Hall/CRC, 2007.
[39] D. Boiroux, R. Juhl, H. Madsen, J.B. Jørgensen, An efficient UD-based algorithm for the computation of maximum likelihood sensitivity of continuous-discrete systems, in: Proceedings of the IEEE Fifty fifth Conference on Decision and Control (CDC), IEEE, 2016, pp. 3048–3053.